© 2020. Published by The Company of Biologists Ltd | Journal of Experimental Biology (2020) 223, jeb212829. doi:10.1242/jeb.212829

RESEARCH ARTICLE

Nanometer-scale structure differences in the myofilament lattice spacing of two cockroach leg muscles correspond to their different functions

Travis Carver Tune[1], Weikang Ma[2], Thomas Irving[2] and Simon Sponberg[1,3,*]

ABSTRACT

Muscle is highly organized across multiple length scales. Consequently, small changes in the arrangement of myofilaments can influence macroscopic mechanical function. Two leg muscles of a cockroach have identical innervation, mass, twitch responses, length–tension curves and force–velocity relationships. However, during running, one muscle is dissipative (a 'brake'), while the other dissipates and produces significant positive mechanical work (bifunctional). Using time-resolved X-ray diffraction in intact, contracting muscle, we simultaneously measured the myofilament lattice spacing, packing structure and macroscopic force production of these muscles to test whether structural differences in the myofilament lattice might correspond to the muscles' different mechanical functions. While the packing patterns are the same, one muscle has 1 nm smaller lattice spacing at rest. Under isometric stimulation, the difference in lattice spacing disappeared, consistent with the two muscles' identical steady-state behavior. During periodic contractions, one muscle undergoes a 1 nm greater change in lattice spacing, which correlates with force. This is the first identified structural feature in the myofilament lattice of these two muscles that shares their whole-muscle dynamic differences and quasi-static similarities.

KEY WORDS: Muscle work loop, X-ray fiber diffraction, *Blaberus discoidalis*

INTRODUCTION

Many biological structures, especially tissues, have hierarchical, multiscale organization (McCulloch, 2016). Of these, muscle is exceptional because it is also active – capable of producing internal stress based on the collective action of billions of myosin motors (Maughan and Vigoreaux, 1999). At the macroscopic scale, muscle can perform many roles in organisms, acting like a motor, brake or spring depending on the task required (Josephson, 1985; Dickinson et al., 2000). It is even possible for different parts of a single muscle to behave with different mechanical functions, defined by their mechanical work and force production (Roberts et al., 1997; George et al., 2013). This function versatility enables muscle's diverse roles in animal locomotion and behavior. Muscle's mechanical function can be difficult to predict, especially under perturbed conditions, because of muscle's hierarchical structure across multiple length scales (Powers et al., 2018; Ahn et al., 2006; Tytell et al., 2018).

Muscle's mechanical function during locomotion is typically characterized through a work loop: a stress–strain (or force–length) curve in which the length (or strain) of the muscle is prescribed through a trajectory and electrically activated at specific phases during the cycle of shortening and lengthening (Josephson, 1985; Ahn, 2012). The area inside the loop gives the net work done by the muscle and can be positive, negative or zero. Work loops that produce zero net work can still have different behavior, being spring-like, isometric and strut-like (Roberts et al., 1997), or biphasic with a period of negative and positive work. Work loop parameters typically mimic either *in vivo* or power-maximizing conditions.

Many other physiological characterizations of muscle are steady state in some respect. Twitch responses are isometric. The length–tension curve is obtained under constant, usually tetanic, stimulation. Even the force–velocity curve is taken as the force at constant activation during constant velocity shortening for a given load. These macroscopic properties arise from and, in fact, helped establish the crossbridge basis for muscle contraction and sliding filament theory (Gordon et al., 1966; Huxley and Simmons, 1971). Although these steady-state macroscopic measurements are important determinants of muscle work loops, they are not sufficient to account for the variability of muscle work output and hence mechanical function under dynamic conditions (Josephson, 1999). The multiscale nature of muscle suggests that subtle differences in structure of the contractile apparatus at the micro to nanometer scale could also be playing an underappreciated role in determining differences in work output and hence macroscopic mechanical function (Williams et al., 2010, 2013; Irving et al., 2000). Here, we determine whether there are structural differences in muscles with functional differences that cannot be explained by classical steady-state measurements

The structural arrangement of actin-containing thin filaments and myosin-containing thick filaments in a sarcomere forms a regular lattice with spacings on the scale of 10s of nanometers (Millman, 1998). This myofilament lattice inside each sarcomere is a crystal in cross-section even under physiological conditions. As a result, its structure can be studied by X-ray diffraction even during force production and length changes (Irving, 2006; Iwamoto, 2018). Here, we use 'lattice spacing' to refer to the distances between the repeating planes of actin and myosin filaments in this lattice. Lattice spacing depends in part on the axial length of the muscle, stemming from the strain placed on the muscle fibers during contraction. However, the filament lattice spacing in muscle also depends on the presence of radial forces, stemming from structural proteins such as

[1]School of Physics, Georgia Institute of Technology, Atlanta, GA, 30332 USA. [2]Biophysics Collaborative Access Team and CSRRI, Department of Biological Sciences, Illinois Institute of Technology, Chicago, IL, 60616 USA. [3]School of Biological Sciences, Georgia Institute of Technology, Atlanta, GA, 30332 USA.

*Author for correspondence (sponberg@gatech.edu)

S.S., 0000-0003-4942-4894

Received 22 August 2019; Accepted 9 March 2020

Journal of Experimental Biology (2020) 223, jeb212829. doi:10.1242/jeb.212829

titin, as well as crossbridge attachment, which can generate radial forces (Bagni et al., 1994; Cecchi et al., 1990) that are of the same order as crossbridge axial forces (Williams et al., 2013).

Differences in lattice structure even at the nanometer scale can have profound effects of force development in muscle. Lattice spacing influences myosin binding probability and hence axial and radial force production (Schoenberg, 1980; Williams et al., 2010; Tanner et al., 2007, 2012). Changing only lattice spacing can enhance Ca^{2+} sensitivity (the shape of force–pCa curves) (Fuchs and Wang, 1996) and change crossbridge kinetics (Adhikari et al., 2004). A change in lattice spacing of just several nanometers even accounts for up to 50% of the force change in a typical muscle's force–length curve (Williams et al., 2013). Temperature differences in insect flight muscle have been shown to change crossbridge binding, lattice spacing and work output (George et al., 2013). What is still unknown is whether myofilament lattice structure (its packing arrangement and spacing) might correspond to macroscopic work in the absence of other differences in physiology, and hence whether differences in lattice structure might be important in the functional role of muscle during locomotion.

To explore the potential significance of structural differences, we looked for two very similar muscles that have unexplained differences in their work production. Two of the femoral extensors of the cockroach *Blaberus discoidalis* are ideal in this respect (Fig. 1A). These two muscles have the same tetanic force–length curves, twitch response, force–velocity curve, phase of activation, force enhancement due to passive pre-stretch, and force depression due to active shortening (Full et al., 1998; Ahn et al., 2006). They are even innervated by the same single, fast-type motor neuron (Becht and Dresden, 1956; Pearson and Iles, 1971) and share the same synaptic transmission properties (Becht et al., 1960), meaning that both muscles are activated as a single motor unit in all conditions. These muscles share the same anatomical and steady-state physiological properties typically used to characterize muscle performance. However, when the two muscles undergo dynamic patterns of strain and activation that match those that they experience during *in vivo* running, one muscle acts like a brake with a dissipative work loop, while the other is more like a motor with a net positive, biphasic work loop (Fig. 1B). It is difficult to reconcile the similarities between these muscles under steady state, and their difference in actual muscle function. Ahn et al. (2006) did observe differences in these muscles' submaximal force–length curves, but only at short lengths, and concluded that these differences alone could not account for the differences in function. Moreover, the origin of these submaximal differences was unknown, although they did suggest that structural differences in the myofilament lattice may account for the differences under dynamic conditions.

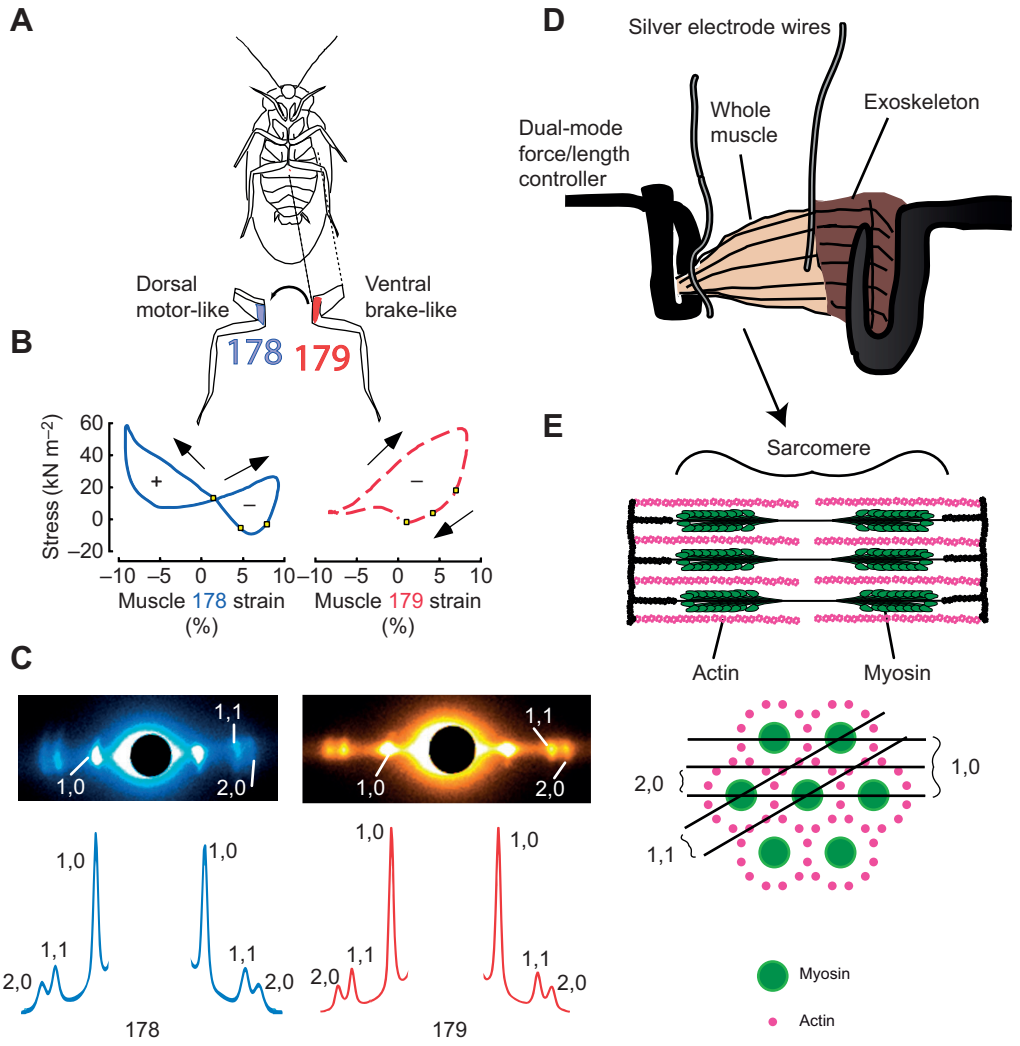

Fig. 1. Schematic diagram representing the anatomy of *Blaberus discoidalis*, and the experimental set up used to obtain x-ray diffraction images of muscles under *in vivo*-like conditions. (A) Ventral view of *Blaberus discoidalis* showing the hind-limb femoral extensors 178 and 179 (notation from Carbonell, 1947). (B) *In situ* work loops performed on muscles 178 and 179 show a difference in function despite near identical steady-state behavior (work loop figures reproduced with permission from Ahn et al., 2006). (C) X-ray diffraction patterns from muscles 178 and 179 with the most prominent peaks labeled. Also shown is the intensity profile along the equatorial axis. (D) A diagram shows the experimental set-up. The X-ray beam path is perpendicular to the contraction axis. (E) Multiscale hierarchy of muscle structure, showing a single sarcomere (1–10 μm) of a muscle (1–10 mm) and the sarcomere cross-section, with diffraction planes (10s of nm) corresponding to the peaks indicated in C. Spacing between diffraction planes in E is related by Bragg's law to the spacing between peaks in C, while the intensity of peaks shown in C is related to the mass lying along depicted planes in E.

Journal of Experimental Biology (2020) 223, jeb212829. doi:10.1242/jeb.212829

Critically, any structural feature that would be consistent with the differences in work output would have to correspond not only to the dynamic differences between the two muscles, but also to their steady-state similarities. We tested two possible, and not mutually exclusive, hypotheses. First, we hypothesized that the myofilament lattice in the two muscles might have a different packing structure. Actin and myosin vary in their ratio and packing pattern across muscles (Millman, 1998; Squire et al., 2005), which can be inferred from how the muscle diffracts X-rays (Irving, 2006). Different packing structures could produce different dynamics of force development, as changing the packing pattern will change the spacing between myosin and actin filaments (Millman, 1998), which changes their binding probability (Williams et al., 2010). Second, we hypothesized that the myofilament lattice spacing might change, but only under dynamic conditions (i.e. work loop conditions that mimic *in vivo* running), while remaining the same during steady-state stimulation. Because of constraints involving simultaneous work loop and X-ray imaging, we cannot exactly replicate the conditions of previous *in situ* work loop studies and must rely on isolated muscle preparations. Nonetheless, we can examine myofilament lattice spacing both during twitches and then during work loop conditions matching those in Ahn et al. (2006) as closely as possible. The overall goal of these hypotheses is to test whether these muscles have structural differences in their actin–myosin lattice, which might be large enough to effect force macroscopic force production and mechanical function. If so, we predict that structural differences must manifest under dynamic conditions, but not under steady-state conditions.

MATERIALS AND METHODS

Animals

Blaberus discoidalis Audinet-Serville 1839 were maintained in a colony at the Georgia Institute of Technology under a 12 h:12 h light:dark cycle and provided food *ad libitum*. Muscles 178 and 179 are located on the mediodorsal and medioventral sides of the coxa, respectively (Ahn et al., 2006). After removing the whole hind-limb, the leg was pinned such that the femur formed a 90 deg angle with the axis of contraction for 178 and 179 with either dorsal or ventral side facing up, which defined the muscles rest length (RL). After removing enough exoskeleton to view the muscle of interest, its rest length was measured from a characteristic colored spot on the apodeme to the anterior side of the coxa, where the muscle originates (Full et al., 1998). We also measured the width of the muscle at mid-length. Once dissected from the coxa, the muscle was mounted between a dual-mode muscle lever (model 305C, Aurora Scientific, Aurora, Canada) and a rigid hook, and length was set to 104.4% RL for muscle 178 and 105% for muscle 179. This is because during *in vivo* running, the mean length of the muscle is not the rest length. We define this as the operating length (OL) of the muscle, or the mean length during *in vivo* running (Ahn et al., 2006; Ahn and Full, 2002). All strain measurements later in the text are relative to this OL. Silver wire electrode leads were placed at opposite ends of the muscle for extracellular activation as in Sponberg et al. (2011a).

Time-resolved X-ray diffraction

Small-angle X-ray fiber diffraction was done using the Biophysics Collaborative Access Team (BioCat) Beamline 18ID at the Advanced Photon Source (APS), Argonne National Laboratory. The beam dimensions at the focus were 60×150 µm, vertically and horizontally, respectively, with a wavelength of 0.103 nm (12 keV). Initial beam intensity is 10^{13} photons s^{-1}, which we attenuated with 12 sheets of 20 µm thick aluminum, about a 65% reduction. For all cases, diffraction images were recorded on a Pilatus3 X 1M pixel array detector (Dectris Inc.) with an exposure time of 4 ms with a 4 ms period between images, during which a fast shutter was closed to reduce radiation damage.

Experimental protocol

After being extracted and mounted, muscles were placed in the beam-line and set to the *in vivo* operating length we measured pre-dissection. We then stimulated with a twitch stimulation pattern consisting of three spikes separated by 10 ms. The three-spike pattern we chose was based on previous work (Ahn et al., 2006; Ahn and Full, 2002) that showed this was the *in vivo* activation pattern during running. Time-resolved X-ray images were taken starting from t=−25 ms, from which we obtained passive isometric measurements, and ending at t=175 ms, with t=0 defining the moment of stimulation. We performed these isometric twitch experiments at mean strain offsets of −10, −5, 0, +5, +10% OL each for both muscles. We estimated cross-sectional area from the diameter of the muscle assuming a cylindrical shape, and used this to calculate stress. The X-ray frame closest to peak stress was used for the active quasistatic measurements. Since these muscles rarely experience tetanic activation *in vivo*, and because repeated tetanic stimulation combined with heat and radiation damage from repeated X-ray imaging would have reduced the viability of each sample, we chose not to examine lattice spacing changes under tetanic stimulation.

Next, we tested the muscles' responses under several different work loop conditions. First, strain amplitude (peak to peak) was 18.5% of OL for muscle 178 and 16.4% of OL for muscle 179. Strain amplitude was different for the two muscles because the muscles are slightly different lengths but must have identical absolute length change during *in vivo* running. The driving frequency was 8 Hz, with activation consisting of three spikes at 6 V at 100 Hz, at a phase of activation of 8%, with 0 defined as the start of shortening. These are the *in vivo* conditions of these muscles during running (Full et al., 1998; Ahn et al., 2006), except with the muscle isolated and extracellularly stimulated. We then changed the oscillation frequency to 11 Hz while keeping the same phase of activation, which matched the conditions from Sponberg et al. (2011a) including the same method of stimulation. We then performed work loops under the same phase of activation, 8 Hz oscillation frequency and amplitude as before but with mean changes in length (offset strain) of −10, −5, 0, +5, +10% OL. We also performed passive work loop measurements for every active work loop condition. Each work loop trial consisted of eight cycles, and we discarded the first cycle. Muscle stress was calculated using the average mass values from Ahn et al. (2006) and the measured resting lengths because these measurements produced less variation than attempts to measure mass following X-ray experiments. During our limited beam time, we gathered data from eight samples of muscle 178 and 10 samples of muscle 179, which were not consistently from the same individual animal. Because prep viability decreases rapidly during prolonged X-ray exposure, not every condition reported has the same number of individuals. Therefore, each figure reports the number of samples that are included in that analysis.

Analysis

The most prominent peaks in the muscle diffraction patterns are the (1,0), (1,1) and (2,0) equatorial peaks, all of which correspond to crystallographic diffraction planes in the muscle crystal lattice (see

Journal of Experimental Biology (2020) 223, jeb212829. doi:10.1242/jeb.212829

Fig. 1C,E). Because the intensity is related to the mass which lies along the associated plane, we can use the (1,1) and (2,0) peaks to determine the arrangement of actin in the lattice. If more mass is located along the (1,1) plane, as in vertebrate muscle, the (1,1) peak will be much brighter than the (2,0) peak, and $I_{11}/I_{20}>>1$ (Irving, 2006). In invertebrate flight muscle, more mass is aligned with the (2,0) plane, which will mean the (2,0) peak is brighter than the (1,1) peak, and $I_{11}/I_{20}<<1$ (Irving, 2006). Also, the spacing between two peaks gives the spacing between the corresponding planes in the lattice via Bragg's law, $\lambda = 2d\frac{s}{L}$, where λ is the wavelength of the X-ray, d is the lattice spacing, s is half the peak to peak distance and L is the sample to detector distance (Irving, 2006). We can use the (1,0) peaks to determine the lattice spacing d_{10}, which is proportional to the inter-myosin distance, and therefore proportional to the distance between thick and thin filaments.

Lattice spacing changes are usually on the order of 1–3 nm (2–5%), necessitating image analysis to resolve them (Irving, 2006). X-ray diffraction patterns were analyzed by automated software (Williams et al., 2015), a subset of which was verified by hand fitting with fityk, a curve-fitting program (Wojdyr, 2010). Individual frames for which the automated software failed to resolve peaks were discarded. Trials with frames that consistently failed during multiple cycles to resolve peaks were discarded totally.

RESULTS

Similarity in packing structure cannot explain functional differences

We first tested whether the two muscles had the same lattice packing structure (Fig. 1E). In invertebrates, there can be a wide variety of actin packing patterns. Two muscles with different myosin–actin ratios and geometry might have similar steady-state behavior because they have the same number of myosin heads available for crossbridge binding, but could have different dynamic behavior as a result of having more or fewer actin filaments. We can use the ratio ($I_{11}/I_{20}=I_{11/20}$) of intensity in the (1,1) and (2,0) peaks (Fig. 1, peaks labeled) to determine whether muscles 178 and 179 have similar packing patterns (see Materials and Methods).

We measured the intensity of the (1,1) and (2,0) peaks of muscles 178 and 179 and found $I_{11/20}$=2.47±0.4 and 2.68±0.4 [mean±95% confidence intervals (CI) of the mean] for muscles 178 and 179, respectively (Fig. 2). Although we have not modeled what packing pattern would produce such an intensity ratio, we know from previous electron microscopy work that muscle 137, the midlimb analog of 179, has a 6:1 packing pattern common among insect limb muscle (Jahromi and Atwood, 1969). The similar ratios (P=0.44, Wilcoxon rank sum test) mean it is likely muscle 179 also has this

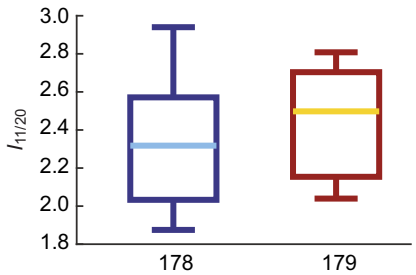

Fig. 2. Boxplots of the intensity ratio $I_{11/20}$ for muscles 178 (n=8, left) and 179 (n=9, right), with median and 25th and 75th percentiles. There is no significant difference between the two muscles' intensity ratios, indicating that they have the same packing pattern (P=0.44, Wilcoxon rank sum test).

packing pattern. Regardless, based on the intensity ratio of muscle 178 compared with muscle 179, we determined that muscle 178 has the same structure as muscle 179. Because the two muscles have the same packing structure, this alone cannot account for their different work loops.

A 1 nm difference in lattice spacing under passive conditions disappears when muscles are activated to steady state

Because we did not observe a difference in packing structure between the two muscles, we next asked whether the lattice spacing under isometric conditions differed between the two muscles. We used the value of d_{10} at peak stress as the steady-state active lattice spacing (Fig. 3). The peak stress values at each strain for both muscles are recorded in Table 1, and passive and active d_{10} are shown.

We found a significant structural difference between the two muscles at rest, but not when activated. Under passive conditions, muscle 178's lattice spacing was 1.01±0.41 nm (mean±95% CI of the mean) smaller than that of muscle 179 across all five strain conditions (P=0.005). When activated, the myofilament lattice of muscle 178 expanded radially by approximately 1 nm (see inset in Fig. 3) under all strain conditions, but activating muscle 179 caused no statistically significant change in lattice spacing at any strain condition (P=0.008 and P=0.52, two-factor ANOVA accounting for activation and strain, for muscles 178 and 179, respectively; Fig. 3). As a result, the two muscles have statistically indistinguishable lattice spacings when both were activated under steady-state conditions (0.05±0.4 nm apart, P=0.86). Taken together, these measurements show that under passive conditions, the lattice spacing of these two muscles is different, but that under quasi-static submaximal conditions, their lattice spacing is the same. This is because the lattice spacing of muscle 178 increased to match muscle 179's lattice spacing, which did not change.

The two muscles have different lattice spacing dynamics

The isometric comparison shows that there is a structural difference between the two muscles under passive conditions which is not manifest under steady-state activation. This is consistent with the two muscles having similar twitch, force–length and force–velocity properties, which are all taken at steady activation. We wanted to see what structural differences might exist under conditions mimicking *in vivo* behavior, so we next examined how lattice spacing behaves during dynamic contractions. We measured d_{10} during passive work loops and work loops at 8 Hz with the *in vivo* activation pattern and phase (see Materials and Methods). When activated, the time course of d_{10} in muscle 178 differed significantly in the active versus the passive case, whereas muscle 179 lattice spacing did not (P=0.008 and P=0.11, respectively, two-factor ANOVA between strain and activation). Fig. 4 shows the mean subtracted 8 Hz results in order to compare the peak-to-peak differences in lattice spacing during active and passive work loops. In both muscles, passive (unstimulated) muscle underwent comparable peak-to-peak lattice spacing change. Activation produced additional lattice spacing expansion of 1.1±.5 nm at the peak stress plateau. Peak lattice spacing change in muscle 179 was 0.4±0.4 nm (see Fig. 5 for a representative lattice spacing, stress and incremental work time series). Therefore, under dynamic conditions, we found that peak-to-peak d_{10} increased more in muscle 178 than in muscle 179 (Fig. 4), continuing the structural motif we found in the steady-state case.

8 Hz and 11 Hz work loops differed in net work

For technical reasons, we could not exactly prepare the muscles in the same ways as in the experiments from Ahn et al. (2006), where

Journal of Experimental Biology (2020) 223, jeb212829. doi:10.1242/jeb.212829

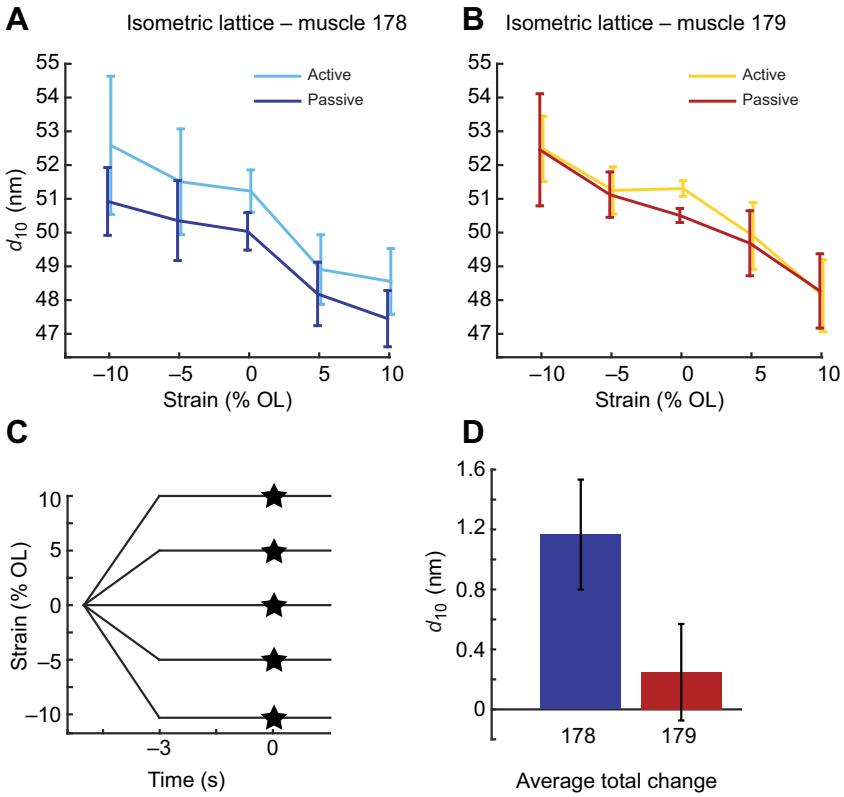

Fig. 3. Lattice spacing changes of muscle 178 and 179 under steady-state isometric conditions. Passive and active d_{10} of muscles 178 (A) and 179 (B) at strains of −10% to +10% of operating length (OL), with 95% confidence interval (CI) of the mean. (C) Strain conditions used, with the timing of activation indicated by the star at t=0. (D) Total average change under activation in d_{10} across all strains with 95% confidence of the mean, showing a difference in the mean of 0.92 nm (P<10^{-3}). Sample sizes, n, at strains (−10,−5,0,5,10) were (7,6,8,7,7) for muscle 178 and (8,9,8,9,9) for muscle 179.

the muscle was left *in situ* in the limb and the motor neuron was directly stimulated. Our preparation required isolating the muscles from the cockroach leg and directly stimulating them with silver wire electrodes (Sponberg et al., 2011a). This was necessary to restrict X-ray imaging to a single muscle and because of size constraints for fitting the experimental apparatus in the beam line. When extracellularly stimulating, muscle force rise times are faster (approximately 8 ms) because of the lack of transmission and synaptic delays, and decrease faster likely because all sarcomeres are simultaneously activated (Sponberg et al., 2011a). Consequently, under identical 8 Hz running conditions, force develops sooner in our muscle preparations than in the neural stimulation, *in situ* work loops of Ahn et al. (2006). As a result, under extracellular stimulation, both muscles 178 and 179 produce small but significant positive work and more negative work (Table 1). In prior experiments, faster 11 Hz running conditions were also implemented in work loops (Sponberg et al., 2011a). In muscle 137, the midleg equivalent of muscle 179, these 11 Hz conditions with extracellular stimulation gave work that was more similar to that of the Ahn et al. (2006) and Full et al. (1998) conditions. The faster frequency reduced stride period correspondingly. To compare with these conditions, we repeated all of our trials with 11 Hz work loops. In this case, we found results more consistent with previous work loops, although the difference between the two muscles was still not as dramatic as those from the Ahn et al. (2006) *in situ* work loops. Muscle 178 produced positive work statistically indistinguishable from the 8 Hz condition (P=0.56, t-test), but muscle 179 produced significantly less work (P=0.017, t-test), and both muscles produced even more negative work than in the 8 Hz conditions (P=0.07 and P=0.002, t-test, for muscles 178 and 179, respectively). The differences in preparation between previous *in situ* work and our isolated muscle protocols are likely the main source of discrepancy. However, negative work also

Table 1. Work done with driving frequencies of 8 Hz and 11 Hz, with mean length, width and peak isometric twitch forces

	Muscle 178		Muscle 179	
8 Hz: work per cycle (active) (J kg^{-1})	Total positive	Total negative	Total positive	Total negative
	0.35±0.11	−1.23±0.30	0.67±0.31	−1.27±0.35
11 Hz: work per cycle (active) (J kg^{-1})	Total positive	Total negative	Total positive	Total negative
	0.46±0.25	−2.95±1.54	0.25±0.12	−3.74±1.08
Length (mm)	3.59±0.20		3.78±0.15	
Width (mm)	2.17±0.28		1.69±0.27	
Stress (mN mm^{-2}) at −10% strain offset	50.9±20.5		60.1±35.4	
Stress (mN mm^{-2}) at −5% strain offset	78.8±29.2		89.7±35.9	
Stress (mN mm^{-2}) at 0% strain offset	101.6±18.8		158.5±22.2	
Stress (mN mm^{-2}) at 5% strain offset	124.0±24.0		166.3±34.8	
Stress (mN mm^{-2}) at 10% strain offset	129.2±27.8		190.4±40.7	

All values are means±95% confidence intervals of the mean. For the 8 Hz conditions, n=6 for muscle 178 and n=7 for muscle 179. For the 11 Hz conditions, n=4 for muscle 178 and n=9 for muscle 179. Stress values are peak stress during isometric conditions under submaximal three spike stimulation pattern. We report total positive and total negative work, rather than net work, to better emphasize the differences between 11 Hz and 8 Hz work loops, and the differences between muscles.

Journal of Experimental Biology (2020) 223, jeb212829. doi:10.1242/jeb.212829

Table 2. Pearson linear correlation coefficient between stress and Δd_{10} of each individual

Muscle	Condition	Correlation coefficient	*P*	Time shift (ms)
178	8 Hz	0.34	$<10^{-2}$	24
		0.47	$<10^{-2}$	16
		0.45	$<10^{-2}$	0
		0.21	0.01	32
		0.77	$<10^{-2}$	–8
178	11 Hz	0.45	$<10^{-2}$	–22.8
		0.35	$<10^{-2}$	–22.8
		0.35	$<10^{-2}$	22.8
		0.16	0.01	53.2
179	8 Hz	0.29	$<10^{-2}$	0
		0.41	$<10^{-2}$	16
		0.46	$<10^{-2}$	16
		0.09	0.2	–40
		0.57	$<10^{-2}$	24
		0.34	$<10^{-2}$	–40
		0.50	$<10^{-2}$	0
179	11 Hz	0.46	$<10^{-2}$	–15.2
		0.48	$<10^{-2}$	15.2
		0.55	$<10^{-2}$	–7.6
		0.41	$<10^{-2}$	30.4
		0.61	$<10^{-2}$	7.6
		0.44	$<10^{-2}$	–22.8

Timing differences are the peak cross correlations for each work loop condition in each individual. Our convention is that negative timing difference indicate stress changes follow Δd_{10}, although conditions are periodic.

has large variation (50–75%) from experiment to experiment, both here (see Table 1) and in previous studies at these conditions (Ahn et al., 2006; Sponberg et al., 2011a), suggesting that there might be a large range of typical responses across individuals.

Lattice spacing dynamics correlate to changes in stress

Given the lattice spacing difference between muscles 178 and 179, we next tested whether these changes correlated to the timing of stress differences in the two muscle's dynamic behavior. The two muscles have nearly identical strain patterns so differences in mechanical work arise from different stress profiles. Given individual variation, we considered the correlations between lattice spacing and stress in every individual from both the 8 Hz and 11 Hz work loops. We paired active and passive work loop conditions for each individual and subtracted the passive spacing changes, which gave us the spacing changes due to activation: $\Delta d_{10}=d_{10,\text{active}}-d_{10,\text{passive}}$. We cross-correlated Δd_{10} with the instantaneous muscle stress (force per cross-sectional area).

In all 8 Hz and 11 Hz trials, changes in lattice spacing from passive to active work loop conditions correlated with stress (see Table 2). We calculated the cross-correlation of lattice spacing and stress and reported the timing difference and correlation coefficient. Fig. 5 shows a representative time series of Δd_{10}, stress (active–passive) and incremental work for muscles 178 and 179 at 8 Hz and 11 Hz. Stimulation occurs just after the start of shortening. Following stimulation, in 8 Hz trials, stress begins to develop in both muscles, but falls off earlier in muscle 179 and plateaus in muscle 178. During this stress plateau, peak Δd_{10} occurs in muscle 178 (Fig. 5A) whereas Δd_{10} in muscle 179 returns to baseline (Fig. 5B). In the 11 Hz trials, stress peaks at the start of shortening in both muscles, which in general is when the peak of Δd_{10} also occurs. However, in the 11 Hz trials, Δd_{10} was sometimes negative during the end of shortening, indicating the lattice spacing decreases from the passive value, although the magnitude of change is still greater in muscle 178 than in muscle 179 (Fig. 5C,D).

Lattice spacing dynamics depend on strain

Under perturbed conditions during locomotion, these muscles can undergo many different strain patterns (Sponberg et al., 2011a; Libby et al., 2020). We next changed the mean strain of the work loop conditions by shifting the mean length by ±5% and +10% of OL. In this way, we tested whether changes in lattice spacing dynamics during the work loops were sensitive to specific length (or strain) trajectories. The midleg homolog to muscle 179 has a large functional range, shifting from a brake to a motor under different activation and strain conditions (Sponberg et al., 2011a). If lattice spacing covaries with work, we might expect corresponding large variations in lattice spacing dynamics under different strain trajectories.

The difference in lattice spacing dynamics between the two muscles was present at every mean offset condition we measured. The peak-to-peak amplitude of d_{10} in muscle 178 always increased during activated work loops compared with passive conditions (Figs 6 and 7). This change was larger than the Δd_{10} for muscle 179 in every case except at −5%, where d_{10} decreased in muscle 179. In many cases, the lattice spacing was actually reduced when the muscle was activated, indicating that activation constrained the radial expansion of the lattice. Overall, the lattice spacing change in muscle 179 is more dependent on the specific length trajectory of the muscle, which is consistent with its variable role as a motor or a brake under perturbed conditions.

DISCUSSION

A single nanometer difference in the myofilament lattice is the first structural difference detected in these otherwise identical muscles that match their function difference in mechanical function and their similar steady-state properties. Before activation, Δd_{10} in muscle 178 has a smaller lattice spacing than muscle 179 by approximately 1 nm at 10% strain, which is where activation occurs *in vivo* (Fig. 8). Simply showing that there is a passive lattice spacing difference is insufficient to explain the two muscles' different work production, because under steady-state (isometric and isotonic) conditions, these two muscles produce the same force. However, stimulation causes muscle 178's lattice spacing to increase, eventually matching that of muscle 179, whereas muscle 179 is already at its steady-state lattice spacing. So muscle 178 has dynamic lattice spacing changes due to activation whereas muscle 179 does not. The 1 nm lattice spacing difference disappears at the plateau of isometric twitches, which is consistent with the identical steady-state macroscopic properties (force–length and force–velocity curves).

During cyclic contractions, where the muscles activate and relax, the muscles' lattice spacing will change both with muscle length (comparable in both muscles) and as they go from passive to activated states. As a result, muscle 178 undergoes a 0.82 nm larger change in lattice spacing during periodic contractions compared with muscle 179. Fig. 8 shows the range of Δd_{10} in order to demonstrate the effect of activation. Because the amount of force that is generated axially is dependent on the lattice spacing, as is the crossbridge binding probability (Schoenberg, 1980; Williams et al., 2010), it is reasonable this increased change in lattice spacing could have functional consequences.

Fig. 8 shows a representation of the lattice spacing changes during activation. At rest, the muscles are offset in lattice spacing (see asterisks in Fig. 8). Under isometric conditions, the lattice spacing in muscle 178 increases while that in muscle 179 does not, leaving them at the same lattice spacing at peak activation (green lines in Fig. 8). During passive, unactivated work loops, lattice spacing changes as a result of axial strain (Fig. 4). We subtracted that

Journal of Experimental Biology (2020) 223, jeb212829. doi:10.1242/jeb.212829

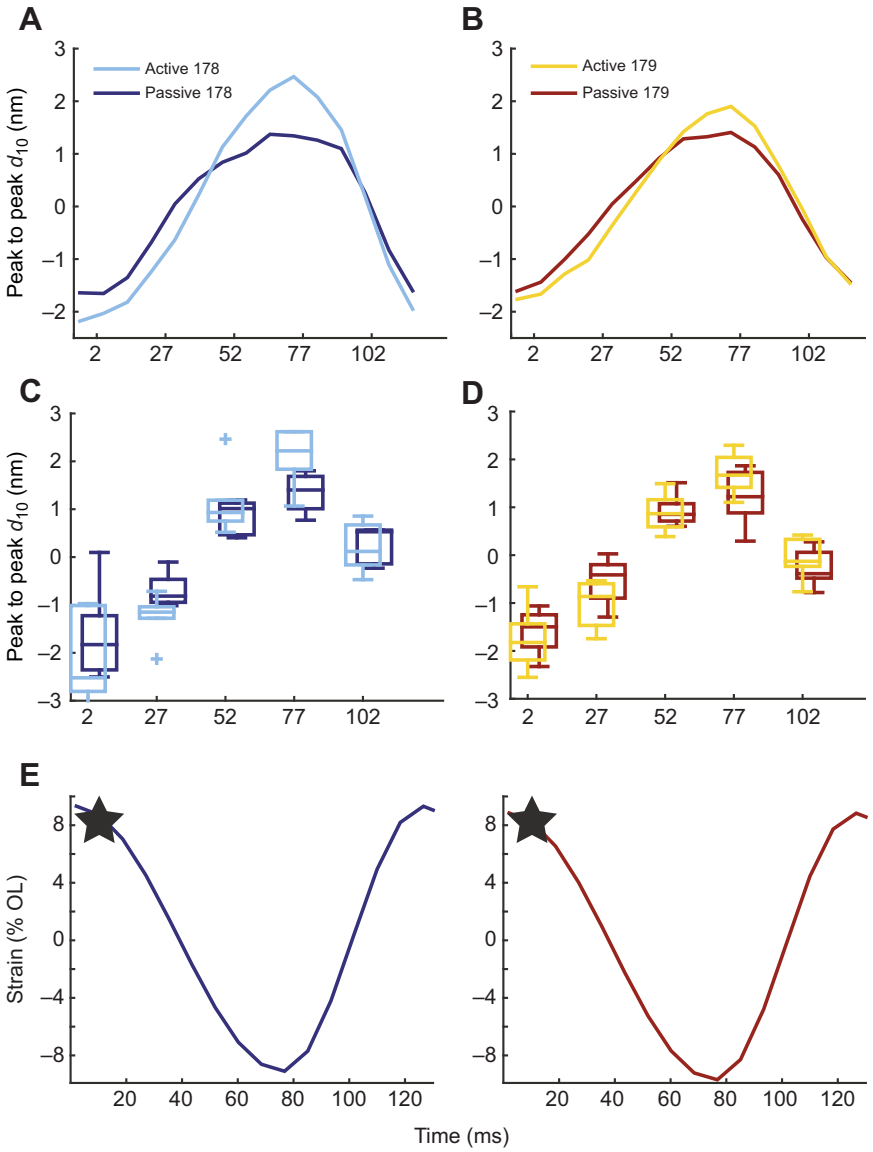

Fig. 4. Lattice spacing changes in muscles 178 and 179 under dynamic, *in vivo*-like conditions mimicking running. (A,B) Mean subtracted active and passive d_{10} lattice spacing for muscles 178 (A) and 179 (B). These were obtained similarly to Fig. 3, but under dynamic work loop conditions. (C,D) Variation in the mean at times corresponding to 0.02*T*, 0.23*T*, 0.43*T*, 0.64*T* and 0.84*T*, which corresponded to the time points nearest maximum strain amplitude $\frac{\Delta L}{L_0}$, $-0.5 \times \frac{\Delta L}{L_0}$, $-0.5 \times \frac{\Delta L}{L_0}$, minimum strain amplitude $\frac{\Delta L}{L_0}$, and 0% strain, respectively, where *T*=120 ms is the cycle period. Boxplots show the median spacing as well as 25th and 75th percentiles, with + indicating data points considered outliers defined as being 1.5 times greater than the interquartile range. Sample sizes are as follows: *n*=5 for passive muscle 178, *n*=6 for active muscle 178, *n*=8 for active and passive muscle 179. (E) Strain trajectories of our work loop protocol for muscles 178 (left) and 179 (right), with the timing of activation indicated by the star.

passive cycling to show the difference in lattice spacing that is due solely to activation of muscle during work loops, Δd_{10} (solid blue and yellow lines). During early shortening (Fig. 8, i to ii) muscle 178 produces more positive work (Table 1), presumably because it is in a more favorable position for myosin heads to bind, and undergoes a larger transient in lattice spacing change (dashed blue to dashed red line, Fig. 8). By the end of shortening (iii) and into lengthening, the myosin heads have bound and the thin filaments (pink) have expanded out to the steady-state value (red dashed line). This expansion is greater in muscle 178 and is likely due to myosin heads producing greater outward radial force in the more constrained configuration. Even though constraints on doing work loops within the X-ray beamline required different methods of stimulation and muscle preparation compared with previous work, changes in lattice spacing correlate with stress production in both muscles 178 and 179 (Fig. 5 and Table 2). The increased transient change in muscle 178's d_{10} after activation corresponds to the plateau in stress development during this portion of the contraction cycle (Fig. 5A). We cannot currently manipulate lattice spacing within intact muscle independent of crossbridge activity to causally connect to muscle function. However, our results suggest structural differences in these two muscles might explain both the dynamic differences and the steady-state similarities of these two cockroach muscles.

Packing structure cannot account for the differences in these two muscles

Although the packing pattern of these two cockroach muscles does not explain their work loop differences, it is still an open question as to how different packing structures might affect muscle function and energetic versatility. Structure indeed does seem to be related to function. In vertebrate muscle [human gastrocnemius (Widrick et al., 2001), rabbit psoas (Hawkins and Bennett, 1995) and frog sartorius (Luther and Squire, 2014), all seen by electron microscopy; and others (Millman, 1998; Squire et al., 2005)], actin is arranged such that one thin filament is located equidistant from three thick filaments, which makes a 1:2 myosin:actin ratio per unit cell. Invertebrate muscle actin packing can vary greatly, with even adjacent muscles in the same animal having different actin arrangement. Flight muscle [*Drosophila* (Irving, 2006); *Lethocerus cordofanus* (Miller and Tregear, 1970)], for example, has one thin filament located equidistant between every two thick filaments,

Journal of Experimental Biology (2020) 223, jeb212829. doi:10.1242/jeb.212829

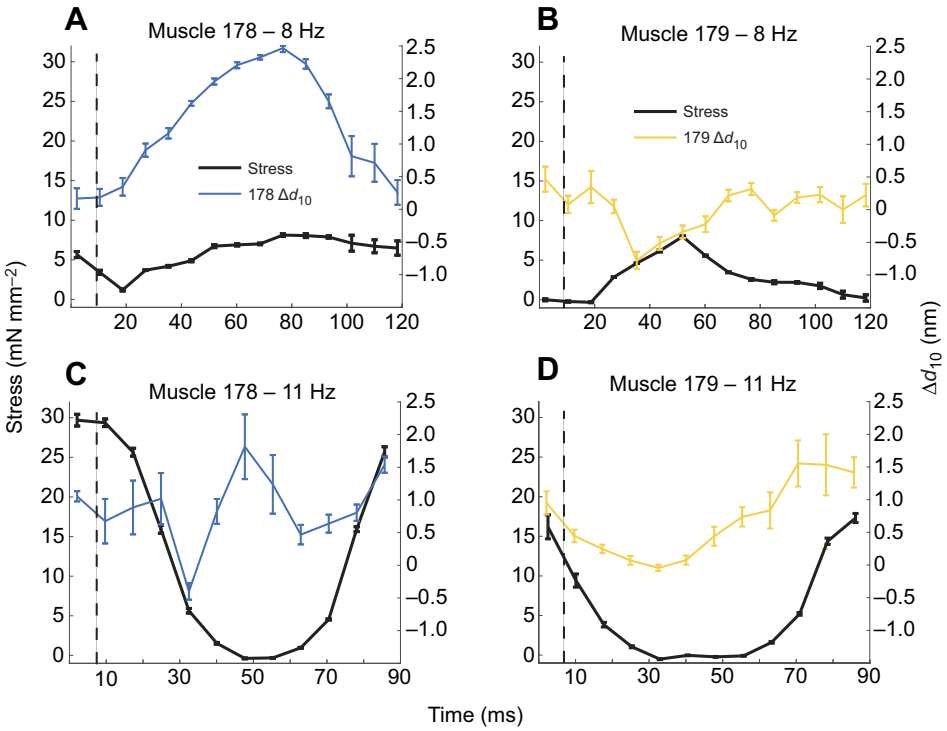

Fig. 5. Example lattice spacing changes (active–passive) and force in muscles 178 and 179 at 8 Hz and 11 Hz. (A) Muscle 178 under 8 Hz work loop conditions. (B) Muscle 179 under 8 Hz work loop conditions. (C) Muscle 178 under 11 Hz work loop conditions. (D) Muscle 179 under 11 Hz work loop conditions. Black solid lines show stress in mN mm^{-2}, colored bars show Δd_{10}, black dashed lines show the timing of stimulation. Lattice spacing changes in 178 were larger for muscle 178 than for muscle 179 under both conditions. Stress under the 11 Hz conditions more closely matched previous results (Ahn et al., 2006), with higher stress during shortening in muscle 178 leading to more positive work than in muscle 179, and both muscles having substantial stress during lengthening, leading to negative work. Under the 11 Hz and 8 Hz conditions, Δd_{10} correlated with stress.

which makes a 1:3 myosin:actin ratio per unit cell, whereas invertebrate limb muscle [crab leg muscle (Yagi and Matsubara, 1977), crayfish leg (April et al., 1971)] has 12 thin filaments surrounding each thick filament, which makes a 1:6 myosin:actin ratio per unit cell. Different packing structures will have different actin–myosin spacing even if d_{10} is the same between muscles because the geometry of actin relative to myosin has changed but myosin geometry has not (Millman, 1998). Different ratios will also affect the availability of actin binding sites for myosin heads. The broad interspecific correlation with muscle locomotor type suggests that packing structure may still be an important determinant of work.

However, in this case, no statistically significant difference was found in the measurements we took of I_{20}/I_{11} for the two muscles and we determined them to have the same ratio and arrangement of myosin to actin filaments. As the muscles are both femoral extensors acting at the same joint, it might seem natural to assume from the beginning that they have the same packing structure. However, even though *B. discoidalis* is flightless, electron micrographs have shown that the largest of the femoral extensors in the middle leg, which is in between the homologs of these two muscles, actually has flight muscle packing arrangement (Jahromi and Atwood, 1969), in which thin filaments are located equidistant between two thick filaments, for a 1:3 myosin to actin filament ratio. Despite being a limb muscle, that femoral extensor is bifunctional and also actuates the wings (Carbonell, 1947). Conversely, a wing actuation muscle in the beetle *Mecynorrhina torquata*, which acts as a steering muscle, has a packing pattern usually associated with limb muscle (Shimomura et al., 2016). So it is not always possible to assume a given packing geometry based only on muscle function. However, in the two muscles considered here, packing structure cannot explain their differences.

Structural differences at the micro-scale could explain functional differences at the macro-scale

It is perhaps surprising that a 1 nm spacing difference could link to such a dramatic functional consequence. Even when we consider the change relative to the absolute lattice spacing of ≈50 nm, it is only a 2% difference (Fig. 3). However, small differences in myofilament configuration can have dramatic effects because of the sensitivity of myosin's spatial orientation relative to its binding site on the thin filament. Crossbridge kinetics depend on lattice spacing and vice versa (Schoenberg, 1980; Adhikari et al., 2004; Tanner et al., 2007; Williams et al., 2013). By undergoing a larger range of lattice spacing during a typical contraction, muscle 178's crossbridge kinetics will likely change more than muscle 179's crossbridge kinetics.

It is not unprecedented for relatively small lattice spacing changes to have multiscale physiological consequences. Temperature has been shown to affect crossbridge activity enough to change d_{10} by as much as 1 nm in hawk moth flight muscle (George et al., 2013). In that case, the temperature difference also corresponds to a functional difference where the cooler superficial part of the muscle acts like a spring while the warmer interior does net positive work (George et al., 2012). In the cockroach muscles there is unlikely to be any temperature difference because both muscles are small and superficial. While the origin of the lattice spacing differences in these muscles is unknown (discussed below), it is reasonable that a 1 nm difference in lattice spacing could influence crossbridge activity enough to make a sizable change in work output. While we do not yet know the full multiscale mechanisms of work differences in these two muscles, we have now shown that there are significant structural differences that correlate with different mechanical functions and are of a magnitude that can impact stress production.

The importance of small nanometer differences in lattice spacing reflects the more general feature of muscle's multiscale nature. Multiscale effects manifest when there is coupling between different length scales and when physiological properties arise that are not predicted by the behavior of other length scales. As myosin crossbridges form, lattice spacing can change as a result of the radial forces generated, aiding or impeding further crossbridge attachment (Williams et al., 2010). Also, crossbridge formation strains myosin

Journal of Experimental Biology (2020) 223, jeb212829. doi:10.1242/jeb.212829

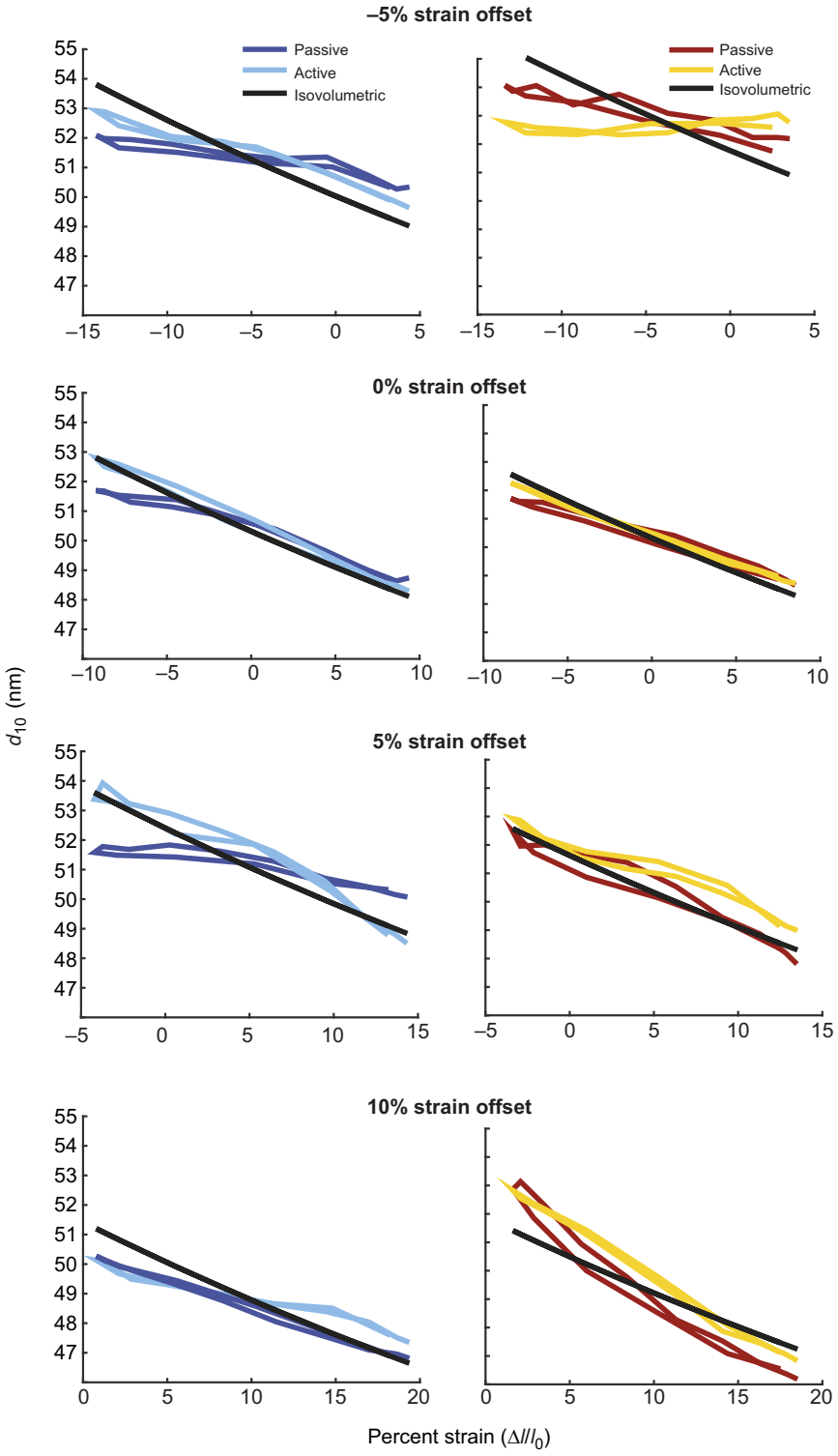

Fig. 6. Lattice loops (d_{10} versus strain) during work loops with mean offsets of −5%, +0%, +5%, +10% operating length (OL) (top to bottom) for muscles 178 and 179 (left and right). The lattice spacing change in passive conditions is due to the axial strain of the myofilament lattice during compression and tension. Under activated conditions, the spacing patterns change in part due to the action of active myosin binding and activation of other proteins, such as titin. Sample size, *n*, for strain conditions (–5,0,5,10) were passive muscle 178, *n*=5 for all strains; active muscle 178, *n*=(5,6,5,5); passive and active muscle 179, *n*=(5,8,8,5). See Fig. 7 for variation in d_{10}.

thick filaments axially, which can influence myosin cooperativity (Tanner et al., 2007). This means crossbridges (10s of nanometer scale) influence and are influenced by the length change of the whole sarcomere (micrometer scale). The deformation of the sarcomere is also a product of strain imposed on the whole muscle fiber (100s of micrometers), which introduces coupling between whole-muscle dynamics and crossbridge kinetics. Spatially explicit models have shown that lattice spacing can affect force, but these models cannot yet predict work under dynamic conditions for a full 3-D lattice (Williams et al., 2010; Tanner et al., 2007). Other detailed half-sarcomere models can capture work differences but cannot yet explicitly incorporate myofilament lattice differences (e.g. Campbell et al., 2011a,b). We generally cannot yet predict mechanical work from steady-state physiological properties, especially during perturbed conditions (Powers et al., 2018; Ahn et al., 2006; Tytell et al., 2018; Libby et al., 2020), but our results link nanometer-scale structural differences with functional differences relevant for locomotion.

Journal of Experimental Biology (2020) 223, jeb212829. doi:10.1242/jeb.212829

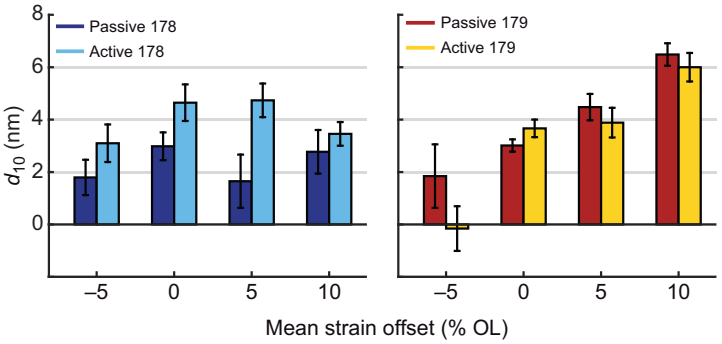

Fig. 7. Mean change in lattice spacing from start of shortening to end of shortening with 95% confidence of the mean for muscles 178 (left) and 179 (right) during passive and active work loops. We found that strain greatly affected lattice spacing for muscle 179 (P<0.001), but not for muscle 178 (P=0.43). In contrast, we found activation greatly affected muscle 178 (P=0.007) but did not significantly affect muscle 179 (P=0.24). Statistics were calculated by two-factor ANOVA (strain and activation). See Fig. 6 for sample sizes.

How might different time courses of lattice spacing arise?

Lattice spacing changes are variable across different muscles, and although the whole muscle is isovolumetric, the myofilament lattice may or may not be (Cecchi et al., 1990). In frog muscles, the lattice is isovolumetric at rest (Matsubara and Elliot, 1972) whereas in active indirect flight muscle, lattice spacing change is minimal (Irving and Maughan, 2000). However, our results show that under some strain conditions (see Fig. 6, 0% and +5% strain offset in muscle 178) even passive muscle is not strictly isovolumetric, and that the lattice spacing increase after activation can make muscles more isovolumetric. This indicates that individual muscles might have different dependencies on length change as well as activation, as we see in Fig. 7.

Many experiments have shown that the relationship between sarcomere length and lattice spacing may be regulated by titin

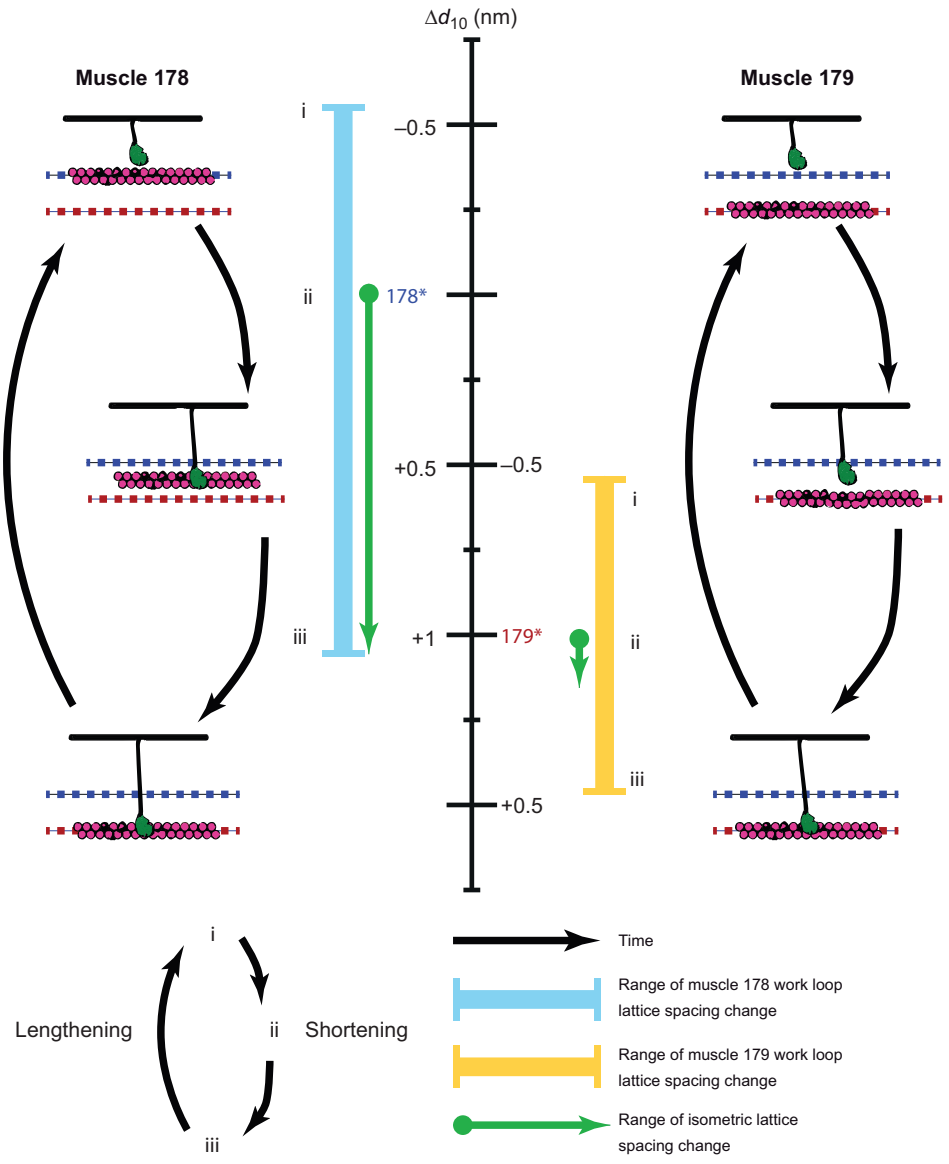

Fig. 8. Lattice spacing has larger dynamic transients in muscle 178 than in muscle 179. Crossbridge schematics on the left and right indicate lattice spacing at different times during a cyclic contraction (i.e. work loop conditions). Times represented by i, ii and iii correspond to the start of shortening (stimulation occurs right after onset), mid-way through shortening, and the transition from shortening to lengthening, respectively. Right before stimulation (i), muscle 178's lattice spacing is tighter (blue dashed line) than muscle 179's (red dashed line). During activation (ii), muscle 178's lattice spacing increases until it reaches the red dashed line (iii), while muscle 179's does not significantly change (see Fig. 3). The muscles then relax during lengthening and the cycle repeats. The central scale bar shows the change in lattice spacing compared with the mean passive lattice spacing at rest for each muscle (indicated by 178* and 179*). These are offset because of the passive differences in the muscle. The green arrows indicate the range of lattice spacing under isometric activation and show that the initial lattice spacing difference disappears at steady state. Both muscles undergo lattice spacing change during periodic contractions because of axial length change. However, muscle 178 has a 0.82 nm larger range in lattice spacing (cyan line) during periodic contractions compared with muscle 179 (yellow line) because of the addition of activation-dependent lattice spacing. Lattice spacing arises from a balance of radial forces from many potential sources, including crossbridges and other sarcomeric proteins (e.g. titin and titin-like molecules; Dutta et al., 2018). Both the amount of force that is generated axially and radially by crossbridges and crossbridge binding rates are dependent on the lattice spacing (Schoenberg, 1980; Williams et al., 2010). These influences could enable even a 1 nm difference to have the potential to drive differences in a muscle's mechanical work output, but we must further explore causal mechanisms.

(Fuchs and Martyn, 2005). For example, by enzymatically lowering the passive tension of titin in mice, it was seen that lattice spacing increased and pCa sensitivity decreased, implying there exists a strong radial component of titin force that influences actin–myosin interaction, possibly by regulating the lattice structure (Cazorla et al., 2001). Bovine left ventricles and left aortas express higher and lower titin stiffness, respectively. Ca^{2+} sensitivity with sarcomere length is much stronger in the ventricle with stiffer titin, and this is coupled with smaller lattice spacing, as seen with X-ray diffraction (Fukuda et al., 2003).

In the muscles in our study, lattice spacing differences might be explained by differences in projectin or sallimus, the titin-like proteins found in insects (Yuan et al., 2015; Bullard et al., 2005, 2006; Burkart et al., 2007). It is possible that the passive radial force component of elastic proteins decreases as muscle strain increases in muscle 179, but remains constant with respect to strain in muscle 178 because lattice spacing change is independent of changes in mean length (mean strain offset) in muscle 178 but not in muscle 179 (Figs 6 and 7). However, titin is thought to become stiffer when activated (Dutta et al., 2018), suggesting a more complicated force balance. Nonetheless, if the stiffness in the projectin or sallimus proteins (the titin analogs in invertebrate muscle; Yuan et al., 2015) increased by different amounts upon activation, crossbridge forces would have different effects on the lattice spacing. If elastic protein stiffness increases under activation in such a way as to balance radial forces generated by bound crossbridges in muscle 179 but not in muscle 178, it could help explain our results.

The offset in filament spacing between the two muscles could also arise from differences in Z disk proteins, such as α-actinin, which cross-link actin (Hooper and Thuma, 2005). While this could account for the passive offset it is less clear how such structural differences in the anchoring of thin filaments alone could explain why the d_{10} difference between the two muscles disappears under steady-state activation. Overall, expansion and contraction of the myofilament lattice arise from a balance of radial forces from many elements.

Structural elements of the actin–myosin lattice have implications for understanding control

In addition to similar muscles producing different magnitudes of mechanical work under comparable conditions, the same muscle can also have a great deal of functional variation. How lattice spacing interplays with macroscopic force production might contribute to how a muscle changes function under perturbed conditions. The way a muscle's lattice spacing changes during periodic contractions at different mean offsets might give clues to how muscles can achieve such versatile mechanical functions. Muscle 179's lattice spacing has a more sensitive dependence on strain (Fig. 6) and a smaller dependence on activation compared with muscle 178 (Fig. 7). On flat terrain while running, this muscle's *in vivo* function is to act as a brake. However, when perturbed, it could perform large amounts of positive work, which can affect center of mass behavior of the whole insect. In muscle 137, the mid-limb analog of muscle 179, a large change in function can arise from small changes in strain and phase of activation which arise from either neural or mechanical feedback (Sponberg et al., 2011a,b). By having lattice spacings with different dependencies on muscle length and activation, different muscles may be able achieve large functional variation such as muscle 137, or be robust in their function even as activation changes.

Conclusions

A 1 nm difference in the spacing of the myofilament lattice is the first feature that matches the steady-state and dynamic similarities and differences in two nearly identical leg muscles in the cockroach. Nanometer size differences in lattice spacing not only influence myosin binding, but also may explain categorical shifts in muscle function that have effects at the scale of locomotion. A single nanometer change in spacing could have this profound effect because of the multiscale coupling from the molecular lattice to the tissue. Simultaneous time-resolved X-ray diffraction and physiological mechanisms are starting to link biophysical differences in muscle structure to macroscopic function even under dynamic conditions.

Acknowledgements

We thank George Steven Chandler and Chidinma Chukwueke for help in data collection, and Sage Malingen, Tom Libby and Tom Daniel for helpful discussions.

Competing interests

The authors declare no competing or financial interests.

Author contributions

Conceptualization: T.C.T., S.S.; Methodology: T.C.T., W.M., T.I., S.S.; Formal analysis: T.C.T., S.S.; Investigation: T.C.T., W.M., S.S.; Resources: T.I.; Data curation: T.C.T.; Writing - original draft: T.C.T., S.S.; Writing - review & editing: T.C.T., W.M., T.I., S.S.; Supervision: T.I., S.S.; Project administration: T.I., S.S.; Funding acquisition: T.I., S.S.

Funding

This work was supported by grant W911NF-14-1-0396 from the Army Research Office. This research used resources of the Advanced Photon Source, a U.S. Department of Energy (DOE) Office of Science User Facility operated for the DOE Office of Science by Argonne National Laboratory under Contract No. DE-AC02-06CH11357. The work was supported by GUP beamtime awards 47291 and 52213. Use of the Pilatus 3 1M detector was provided by grant 1S10OD018090-01 from the National Institute of General Medical Sciences (NIGMS). This project was also supported by grant 9 P41 GM103622 from NIGMS. The content is solely the responsibility of the authors and does not necessarily reflect the official views of the National Institute of General Medical Sciences or the National Institutes of Health. Deposited in PMC for release after 12 months.

Data availability

Data are available from the Dryad Digital Repository (Tune et al., 2020): 978406.

References

Adhikari, B. B., Regnier, M., Rivera, A. J., Kreutziger, K. L. and Martyn, D. A. (2004). Cardiac length dependence of force and force redevelopment kinetics with altered cross-bridge cycling. *Biophys. J.* **87**, 1784-1794. doi:10.1529/biophysj.103.039131

Ahn, A. N. (2012). How muscles function – the work loop technique. *J. Exp. Biol.* **215**, 1051-1052. doi:10.1242/jeb.062752

Ahn, A. N. and Full, R. J. (2002). A motor and a brake: two leg extensor muscles acting at the same joint manage energy differently in a running insect. *J. Exp. Biol.* **205**, 379-389.

Ahn, A. N., Meijer, K. and Full, R. J. (2006). *In situ* muscle power differs without varying *in vitro* mechanical properties in two insect leg muscles innervated by the same motor neuron. *J. Exp. Biol.* **209**, 3370-3382. doi:10.1242/jeb.02392

April, E. W., Brandt, P. W. and Elliott, G. F. (1971). The myofilament lattice: studies on isolated fibers. *J. Cell Biol.* **51**, 72-82. doi:10.1083/jcb.51.1.72

Bagni, M. A., Cecchi, G., Griffiths, P. J., Maeda, Y., Rapp, G. and Ashley, C. C. (1994). Lattice spacing changes accompanying isometric tension development in intact single muscle fibers. *Biophys. J.* **67**, 1965-1975. doi:10.1016/S0006-3495(94)80679-4

Becht, G. and Dresden, D. (1956). Physiology of the locomotory muscles in the cockroach. *Nature* **177**, 836-837. doi:10.1038/177836a0

Becht, G., Hoyle, G. and Usherwood, P. N. R. (1960). Neuromuscular transmission in the coxal muscles of the cockroach. *J. Insect Physiol.* **4**, 191-201. doi:10.1016/0022-1910(60)90026-3

Bullard, B., Burkart, C., Labeit, S. and Leonard, K. (2005). The function of elastic proteins in the oscillatory contraction of insect flight muscle. *J. Muscle Res. Cell Motil.* **26**, 479-485. doi:10.1007/s10974-005-9032-7

Bullard, B., Garcia, T., Benes, V., Leake, M. C., Linke, W. A. and Oberhauser, A. F. (2006). The molecular elasticity of the insect flight muscle proteins projectin

and kettin. *Proc. Natl Acad. Sci. USA* **103**, 4451-4456. doi:10.1073/pnas.0509016103
Burkart, C., Qiu, F., Brendel, S., Benes, V., Hååg, P., Labeit, S., Leonard, K. and Bullard, B. (2007). Modular proteins from the *Drosophila* sallimus (sls) gene and their expression in muscles with different extensibility. *J. Mol. Biol.* **367**, 953-969. doi:10.1016/j.jmb.2007.01.059
Campbell, S. G., Hatfield, C. and Campbell, K. S. (2011a). A model with heterogeneous half-sarcomeres exhibits residual force enhancement after active stretch. *Biophys. J.* **100**, 12a. doi:10.1016/j.bpj.2010.12.277
Campbell, S. G., Hatfield, P. C. and Campbell, K. S. (2011b). A mathematical model of muscle containing heterogeneous half-sarcomeres exhibits residual force enhancement. *PLoS Comput. Biol.* **7**, e1002156. doi:10.1371/journal.pcbi.1002156
Carbonell, C. S. (1947). The thoracic muscles of the cockroach *Periplaneta americana* (L.). *Smithsonian Miscellaneous Collections* **107**, 1-23.
Cazorla, O., Wu, Y., Irving, T. and Granzier, H. (2001). Titin-based modulation of calcium sensitivity of active tension in mouse skinned cardiac myocytes. *Circ. Res.* **88**, 1028-1035. doi:10.1161/hh1001.090876
Cecchi, G., Bagni, M., Griffiths, P., Ashley, C. and Maeda, Y. (1990). Detection of radial crossbridge force by lattice spacing changes in intact single muscle fibers. *Science* **250**, 1409-1411. doi:10.1126/science.2255911
Dickinson, M. H., Farley, C. T., Full, R. J., Koehl, M. A., Kram, R. and Lehman, S. (2000). How animals move: an integrative view. *Science* **288**, 100-106. doi:10.1126/science.288.5463.100
Dutta, S., Tsiros, C., Sundar, S. L., Athar, H., Moore, J., Nelson, B., Gage, M. J. and Nishikawa, K. (2018). Calcium increases titin n2a binding to f-actin and regulated thin filaments. *Sci. Rep.* **8**, 14575. doi:10.1038/s41598-018-32952-8
Fuchs, F. and Martyn, D. A. (2005). Length-dependent Ca^{2+} activation in cardiac muscle: some remaining questions. *J. Muscle Res. Cell Motil.* **26**, 199-212. doi:10.1007/s10974-005-9011-z
Fuchs, F. and Wang, Y.-P. (1996). Sarcomere length versus interfilament spacing as determinants of cardiac myofilament Ca^{2+} sensitivity and Ca^{2+} binding. *J. Mol. Cell. Cardiol.* **28**, 1375-1383. doi:10.1006/jmcc.1996.0129
Fukuda, N., Wu, Y., Farman, G., Irving, T. C. and Granzier, H. (2003). Titin isoform variance and length dependence of activation in skinned bovine cardiac muscle. *J. Physiol.* **553**, 147-154. doi:10.1113/jphysiol.2003.049759
Full, R. J., Stokes, D. R., Ahn, A. N. and Josephson, R. K. (1998). Energy absorption during running by leg muscles in a cockroach. *J. Exp. Biol.* **201**, 997-1012.
George, N. T., Sponberg, S. and Daniel, T. L. (2012). Temperature gradients drive mechanical energy gradients in the flight muscle of *Manduca sexta*. *J. Exp. Biol.* **215**, 471-479. doi:10.1242/jeb.062901
George, N. T., Irving, T. C., Williams, C. D. and Daniel, T. L. (2013). The cross-bridge spring: can cool muscles store elastic energy? *Science* **340**, 1217-1220. doi:10.1126/science.1229573
Gordon, A. M., Huxley, A. F. and Julian, F. J. (1966). The variation in isometric tension with sarcomere length in vertebrate muscle fibres. *J. Physiol.* **184**, 170-192. doi:10.1113/jphysiol.1966.sp007909
Hawkins, C. J. and Bennett, P. M. (1995). Evaluation of freeze substitution in rabbit skeletal muscle. comparison of electron microscopy to x-ray diffraction. *J. Muscle Res. Cell Motil.* **16**, 303-318. doi:10.1007/BF00121139
Hooper, S. L. and Thuma, J. B. (2005). Invertebrate muscles: muscle specific genes and proteins. *Physiol. Rev.* **85**, 1001-1060. doi:10.1152/physrev.00019.2004
Huxley, A. F. and Simmons, R. M. (1971). Proposed mechanism of force generation in striated muscle. *Nature* **233**, 533-538. doi:10.1038/233533a0
Irving, T. C. (2006). X-ray diffraction of indirect flight muscle from *Drosophila in vivo*. In *Nature's Versatile Engine: Insect Flight Muscle Inside and Out* (ed. J. Vigoreaux), pp. 197-211. Landes Bioscience.
Irving, T. C. and Maughan, D. W. (2000). *In vivo* X-ray diffraction of indirect flight muscle from Drosophila melanogaster. *Biophys. J.* **78**, 2511-2515. doi:10.1016/S0006-3495(00)76796-8
Irving, T. C., Konhilas, J., Perry, D., Fischetti, R. and de Tombe, P. P. (2000). Myofilament lattice spacing as a function of sarcomere length in isolated rat myocardium. *Am. J. Physiol.* **279**, H2568-H2573. doi:10.1152/ajpheart.2000.279.5.H2568
Iwamoto, H. (2018). Synchrotron radiation x-ray diffraction techniques applied to insect flight muscle. *Int. J. Mol. Sci.* **19**, E1748. doi:10.3390/ijms19061748
Jahromi, S. S. and Atwood, H. L. (1969). Structural features of muscle fibers in the cockroach leg. *J. Insect Physiol.* **15**, 2255-2262. doi:10.1016/0022-1910(69)90242-X
Josephson, R. K. (1985). Mechanical power output from striated-muscle during cyclic contraction. *J. Exp. Biol.* **114**, 493-512.
Josephson, R. K. (1999). Dissecting muscle power output. *J. Exp. Biol.* **202**, 3369-3375.
Libby, T., Chukwueke, C. and Sponberg, S. (2020). History-dependent perturbation response in limb muscle. *J. Exp. Biol.* **223**, jeb199018. doi:10.1242/jeb.199018
Luther, P. and Squire, J. (2014). The intriguing dual lattices of the myosin filaments in vertebrate striated muscles: evolution and advantage. *Biology* **3**, 846-865. doi:10.3390/biology3040846
Matsubara, I. and Elliot, G. F. (1972). X-ray diffraction studies on skinned single fibres of frog skeletal muscle. *J. Mol. Biol.* **72**, 657-669. doi:10.1016/0022-2836(72)90183-0
Maughan, D. W. and Vigoreaux, J. O. (1999). An integrated view of insect flight muscle: genes, motor molecules, and motion. *Physiology* **14**, 87-92. doi:10.1152/physiologyonline.1999.14.3.87
McCulloch, A. D. (2016). Systems biophysics: multiscale biophysical modeling of organ systems. *Biophys. J.* **110**, 1023-1027. doi:10.1016/j.bpj.2016.02.007
Miller, A. and Tregear, R. T. (1970). Evidence concerning crossbridge attachment during muscle contraction. *Nature* **226**, 1060-1061. doi:10.1038/2261060a0
Millman, B. (1998). The filament lattice of striated muscle. *Physiol. Rev.* **78**, 359-391. doi:10.1152/physrev.1998.78.2.359
Pearson, K. G. and Iles, J. F. (1971). Innervation of coxal depressor muscles in the cockroach, *Periplaneta americana*. *J. Exp. Biol.* **54**, 215-232.
Powers, J. D., Williams, C. D., Regnier, M. and Daniel, T. L. (2018). A spatially explicit model shows how titin stiffness modulates muscle mechanics and energetics. *Integr. Comp. Biol.* **58**, 186-193. doi:10.1093/icb/icy055
Roberts, T. J., Marsh, R. L., Weyand, P. G. and Taylor, C. R. (1997). Muscular force in running turkeys: the economy of minimizing work. *Science* **275**, 1113-1115. doi:10.1126/science.275.5303.1113
Schoenberg, M. (1980). Geometrical factors influencing muscle force development. II. Radial forces. *Biophys. J.* **30**, 69-77. doi:10.1016/S0006-3495(80)85077-6
Shimomura, T., Iwamoto, H., Vo Doan, T. T., Ishiwata, S., Sato, H. and Suzuki, M. (2016). A beetle flight muscle displays leg muscle microstructure. *Biophys. J.* **111**, 1295-1303. doi:10.1016/j.bpj.2016.08.013
Sponberg, S., Libby, T., Mullens, C. and Full, R. (2011a). Shifts in a single muscle's control potential of body dynamics are determined by mechanical feedback. *Philos. Trans. R. Soc. B* **366**, 1606-1620. doi:10.1098/rstb.2010.0368
Sponberg, S., Spence, A. J., Mullens, C. H. and Full, R. J. (2011b). A single muscle's multifunctional control potential of body dynamics for postural control and running. *Philos. Trans. R. Soc. B* **366**, 1592-1605. doi:10.1098/rstb.2010.0367
Squire, J. M., Al-khayat, H. A., Knupp, C. Luther, P. K. (2005). Molecular architecture in muscle contractile assemblies. In *Fibrous Proteins: Muscle and Molecular Motors, Vol. 71 Advances in Protein Chemistry* (ed. J. M. Squire and D. A. D. Parry), pp. 17-87. Academic Press.
Tanner, B. C. W., Daniel, T. L. and Regnier, M. (2007). Sarcomere lattice geometry influences cooperative myosin binding in muscle. *PLoS Comput. Biol.* **3**, 1195-1211. doi:10.1371/journal.pcbi.0030115
Tanner, B. C., Farman, G. P., Irving, T. C., Maughan, D. W., Palmer, B. M. and Miller, M. S. (2012). Thick-to-thin filament surface distance modulates cross-bridge kinetics in *Drosophila* flight muscle. *Biophys. J.* **103**, 1275-1284. doi:10.1016/j.bpj.2012.08.014
Tune, T. C., Ma, W., Irving, T. and Sponberg, S. (2020). Data from: Nanometer-scale structure differences in the myofilament lattice spacing of two cockroach leg muscles correspond to their different functions. *Dryad Dataset* 978406. doi:10.5061/dryad.978406n
Tytell, E. D., Carr, J. A., Danos, N., Wagenbach, C., Sullivan, C. M., Kiemel, T., Cowan, N. J. and Ankarali, M. M. (2018). Body stiffness and damping depend sensitively on the timing of muscle activation in lampreys. *Integr. Comp. Biol.* **58**, 860-873. doi:10.1093/icb/icy042
Widrick, J. J., Romatowski, J. G., Norenberg, K. M., Knuth, S. T., Bain, J. L. W., Riley, D. A., Trappe, S. W., Trappe, T. A., Costill, D. L. and Fitts, R. H. (2001). Functional properties of slow and fast gastrocnemius muscle fibers after a 17-day spaceflight. *J. Appl. Physiol.* **90**, 2203-2211. doi:10.1152/jappl.2001.90.6.2203
Williams, C. D., Regnier, M. and Daniel, T. L. (2010). Axial and radial forces of crossbridges depend on lattice spacing. *PLoS Comput. Biol.* **6**, 1-10. doi:10.1371/journal.pcbi.1001018
Williams, C. D., Salcedo, M. K., Irving, T. C., Regnier, M. and Daniel, T. L. (2013). The length–tension curve in muscle depends on lattice spacing. *Proc. Biol. Sci. R. Soc.* **280**, 20130697-20130697. doi:10.1098/rspb.2013.0697
Williams, C. D., Balazinska, M. and Daniel, T. L. (2015). Automated analysis of muscle X-ray diffraction imaging with MCMC. In *Biomedical Data Management and Graph Online Querying*, pp. 126-133. Springer.
Wojdyr, M. (2010). Fityk: a general-purpose peak fitting program. *J. Appl. Crystallogr.* **43**, 1126-1128. doi:10.1107/S0021889810030499
Yagi, N. and Matsubara, I. (1977). The equatorial x-ray diffraction patterns of crustacean striated muscles. *J. Mol. Biol.* **117**, 797-803. doi:10.1016/0022-2836(77)90070-5
Yuan, C.-C., Ma, W., Schemmel, P., Cheng, Y.-S., Liu, J., Tsaprailis, G., Feldman, S., Southgate, A. A. and Irving, T. C. (2015). Elastic proteins in the flight muscle of *Manduca sexta*. *Arch. Biochem. Biophys.* **568**, 16-27. doi:10.1016/j.abb.2014.12.033